ELSEVIER

Bone 39 (2006) 922–931

BONE

www.elsevier.com/locate/bone

Silk based biomaterials to heal critical sized femur defects

L. Meinel [a,b,c,*], O. Betz [d], R. Fajardo [e], S. Hofmann [a,b], A. Nazarian [e], E. Cory [e], M. Hilbe [f], J. McCool [g], R. Langer [c], G. Vunjak-Novakovic [c,h], H.P. Merkle [b], B. Rechenberg [i], D.L. Kaplan [a], C. Kirker-Head [g]

[a] *Departments of Biomedical Engineering and Chemical and Biological Engineering, Tufts University, Medford, MA 02155, USA*
[b] *Department of Chemistry and Applied Biosciences, ETH Zurich, Switzerland*
[c] *Division of Health Sciences and Technology, Massachusetts Institute of Technology, Cambridge, MA 02142, USA*
[d] *Center for Molecular Orthopaedics, Brigham and Women's Hospital, Harvard Medical School, Boston, MA 02115, USA*
[e] *Orthopaedic Biomechanics Laboratory, Beth Israel Deaconess Medical Center, Harvard Medical School, Boston, MA 02215, USA*
[f] *Institute of Veterinary Pathology, Vetsuisse Faculty, University of Zurich, Zurich, Switzerland*
[g] *Tufts Cummings School of Veterinary Medicine, North Grafton, MA 01536, USA*
[h] *Department for Bioengineering, Columbia University, New York, NY 10032, USA*
[i] *Musculoskeletal Research Unit, Faculty of Veterinary Medicine, University of Zurich, Switzerland*

Received 3 December 2005; revised 31 March 2006; accepted 5 April 2006
Available online 6 June 2006

Abstract

Bone auto- and allografts have inherent drawbacks, therefore the treatment of non-unions and critical size defects in load bearing long bones would benefit from the use of osteopromotive biodegradable, biocompatible and mechanically durable matrices to enhance migration or delivery of cell populations and/or morphogens/cytokines. Silk fibroin biomaterial scaffolds were evaluated as osteopromotive matrices in critical sized mid-femoral segmental defects in nude rats. Four treatment groups were assessed over 8 weeks in vivo: silk scaffolds (SS) with human mesenchymal stem cells (hMSCs) that had previously been differentiated along an osteoblastic lineage in vitro (group I; pdHMSC/SS); SS with undifferentiated hMSCs (group II; udHMSC/SS); SS alone (group III; SS); and empty defects (group IV). When hMSCs were cultured in vitro in osteogenic medium for 5 weeks, bone formation was characterized with bimodal peak activities for alkaline phosphatase at 2 and 4 weeks. Calcium deposition started after 1 week and progressively increased to peak at 4 weeks, reaching cumulative levels of deposited calcium at 16 μg per mg scaffold wet weight. In vivo osteogenesis was characterized by almost bridged defects with newly formed bone after 8 weeks in group I. Significantly ($P<0.01$) greater bone volumes were observed with the pdHMSC/SS (group I) implants than with groups II, III or IV. These three groups failed to induce substantial new bone formation and resulted in the ingrowth of cells with fibroblast-like morphology into the defect zone. The implantation of pdHMSC/SS resulted in significantly ($P<0.05$) greater maximal load and torque when compared to the other treatment regimens. The pdHMSC/SS implants demonstrated osteogenic ability in vitro and capacity to thrive towards the healing of critical size femoral segmental defects in vivo. Thus, these new constructs provide an alternative protein-based biomaterial for load bearing applications.

Keywords: Human mesenchymal stem cells; Silk implant; Tissue engineering; Long bone defect; Mechanical characterization; Micro-computed tomography

Introduction

The clinical need for bone replacement is expected to increase, due in part to the substantial rise in the elderly population of the western world [1,2]. Currently, close to 1 million bone grafts are performed each year for the purpose of skeletal augmentation [3–7]. Autografts remain the clinical gold standard, driving bone repair by providing host cells, growth factors, and a template for bone regeneration. Unfortunately, donor site morbidity, cosmetic concerns, and prolonged hospitalization are just a few of the drawbacks of this procedure [8]. Similarly, the use of allografts presents risks due to immune rejection and disease transmission [9,10]. Orthopedic surgeons would therefore benefit from the

* Corresponding author. ETH Zurich, Department for Chemistry and Applied Biosciences, HCI J 390.1, Wolfgang-Pauli-Str. 10, CH-8093 Zurich, Switzerland. Fax: +41 44 6331314.
E-mail address: lorenz.meinel@pharma.ethz.ch (L. Meinel).

8756-3282/$ - see front matter © 2006 Elsevier Inc. All rights reserved.
doi:10.1016/j.bone.2006.04.019

introduction of osteopromotive scaffolds that could be used to enhance migration and/or delivery of osteogenic cells and cytokines. These materials should combine essential characteristics including biocompatibility, porosity, and appropriate mechanical properties [11–14].

The use of mechanically robust 3D scaffolds offers additional options to more traditional fixation or cast methods to regenerate damaged bone tissue. A major advantage of a mechanically robust matrix is that it is less likely to undergo deformation caused by adjacent tissues (i.e., muscle) at the implant site. This deformation can be a problem, leading to the implant becoming compressed within the defect or even displaced beyond the borders of the defect site, giving rise to the potential for heterotopic bone. Several studies have shown that hMSCs can differentiate along an osteogenic lineage and form three-dimensional bone-like tissue but also detail limitations. Some scaffolds (e.g., calcium phosphate) are characterized with a slow degradation [15], while others degrade too fast [16]. Polymeric scaffolds used for bone tissue engineering, such as poly(lactic-*co*-glycolic acid) or poly-L-lactic acid, can induce inflammation due to the acidity of their hydrolysis products [6,17]. Moreover, matching mechanical properties of native bone remains an issue with most polyesters [7,18]. Therefore, there is a need to identify alternate biomaterials to overcome these limitations and meet the challenging combination of biological, mechanical, and degradation features for bone tissue engineering.

Silk-fibroin-based porous biomaterial scaffolds may contribute to this important niche in biomaterials applications. These scaffolds have low immunogenicity when properly separated from immunogenic and glycosylated proteins [19–22]. Furthermore, they can be produced in a variety of formats including electrospun nets, three-dimensional scaffolds, or tendon-like structures [23–29]. Silks represent the strongest and toughest naturally occurring polymer materials, and recently developed production processes enable the formation of silk biomaterials with decreased content of crystalline β-sheets [27]. This allows for the maintenance of desirable mechanical properties, but more closely regulates the degradation/resorption rates, which can range from weeks to years.

Silk biomaterials have recently been shown to be suitable substrates for the in vitro engineering of bone-like and cartilage-like tissues derived from human mesenchymal stem cells (hMSCs) [30–33]. Interestingly, the geometry of the deposited bone could be reproducibly controlled as a function of scaffold design, shifting bone structures between trabecular-like bone tissue and more plate-like or cortical-like bone [33]. The results of this research have demonstrated that silk fibroin scaffolds promoted bone formation in critical sized cranial defects in mice when seeded with hMSCs predifferentiated in osteogenic medium for 5 weeks (pdHMSC/SS). Bone formation occurred to a much lesser extent when undifferentiated hMSCs (udHMSC) were seeded on the silk scaffolds and minimal bone formation occurred when unseeded silk scaffolds were implanted alone [33].

In the present study, we build on prior studies with non-loaded cranial defects by implanting seeded and unseeded silk scaffolds in load bearing segmental defects in rat femurs. Starting off from detailing the isolated and expanded cell pool used for seeding of the silk scaffolds and a characterization of the events leading to in vitro formation of tissue-engineered bone, the goal of this study was to characterize the healing of the implanted femoral segmental defects after implantation of this system by histology and immunohistochemistry, micro-computed tomography, morphometric quantification of bone formation, and mechanical characterization.

Materials and methods

Materials

Fetal bovine serum (FBS), RPMI 1640 medium, Dulbecco's Modified Eagle Medium (DMEM), basic fibroblast growth factor (bFGF), transforming growth factor-β1 (TGF-β1), penicillin and streptomycin (Pen–Strep), Fungizone, non-essential amino acids (NEAA, consisting of 8.9 mg/l L-alanine, 13.21 mg/l L-asparagine, 13.3 mg/l L-aspartic acid, 14.7 mg/l L-glutamic acid, 7.5 mg/l glycine, 11.5 mg/l L-proline, 10.5 mg/l L serine), and trypsin were from Gibco (Carlsbad, CA). Ascorbic acid-2-phosphate, Histopaque-1077, insulin, and dexamethasone were from Sigma (St. Louis, MO). 1-Ethyl-3-(dimethylaminopropyl) carbodiimide hydrochloride (EDC) and *N*-hydroxy-succinimide (NHS) were purchased from Pierce (Rockford, IL). All other substances were obtained from Sigma. Silkworm cocoons were kindly supplied by M. Tsukada, Institute of Sericulture, Tsukuba, Japan, and Marion Goldsmith, University of Rhode Island. BMP-2 was kindly supplied by Wyeth Biopharmaceuticals, Andover, MA.

Scaffold preparation and characterization

Silk fibroin scaffolds were prepared as described previously [30,31,34]. Cocoons from *Bombyx mori* were boiled for 1 h in an aqueous solution of 0.02 M Na_2CO_3 and rinsed with water to extract sericin. Purified silk was solubilized in 9 M LiBr solution and dialyzed (Pierce, MWCO 2000 g/mol) first against PBS for 1 day and then against 0.1 M 2-(*N*-morpholino)ethanesulfonic acid buffer (MES), 0.5 M NaCl, pH 6, for 1 day. To attach RGD sequences, silk fibroin solution was coupled with GRGDS peptide as previously described [28]. Briefly, the COOH groups on silk were first activated by reaction with EDC/NHS for 15 min at room temperature. To quench the EDC, 70 μl/ml β-mercaptoethanol was added. The solution was then incubated with 0.5 g/l peptide for 2 h at room temperature. The reaction was stopped with 10 mM hydroxylamine. Purified silk fibroin was dialyzed against 0.1 M MES, pH 4.5–5, for 1 day, lyophilized and redissolved in hexafluoro-2-propanol (HFIP) to obtain a 17% (w/v) solution. Granular NaCl (diameter 200–300 μm) was weighed in a Teflon container, and silk/HFIP solution was added at a ratio of 20:1 (NaCl/silk). HFIP was allowed to evaporate for 2 days, and NaCl/silk blocks were immersed in 90% (v/v) methanol for 30 min to induce a protein conformational transition to β-sheet [28]. Blocks were removed, dried and NaCl were extracted by incubation in water for 2 days. Disk shaped scaffolds (8 mm diameter, 2 mm thick) were prepared using a dermal punch (Miltey, Lake Success, NY) and autoclaved at 121°C for 15 min; autoclaving does not alter the structure or shape of the scaffolds.

Cell isolation, expansion, and characterization

Human mesenchymal stem cells (hMSCs) were isolated by density gradient centrifugation from 25 cm^3 whole bone marrow obtained from Clonetics (Santa Rosa, CA). Ten milliliters of aliquots of bone marrow were diluted in 100 ml of isolation medium (RPMI 1640 supplemented with 5% FBS). Twenty milliliters of aliquots of this suspension were overlaid onto a poly-sucrose gradient (δ=1.077 g/cm^3, Histopaque, Sigma, St. Louis, MO) and centrifuged at 800×*g* for 30 min at room temperature. The cell layer was carefully removed, washed in 10 ml isolation medium, pelleted at 300×*g*, and the contaminating red blood cells were lysed in 5 ml of Pure-Gene Lysis solution. Cells were pelleted and suspended in *expansion medium* (DMEM, 10% FBS, Pen–Strep, Fungizone, NEAA, and 1 ng/ml bFGF) and seeded in 175 cm^2 flasks at a density of 5×10^4 cells/cm^2. The adherent cells were allowed to reach approximately 80% confluence (12–17 days for the first passage). Cells were

trypsinized and replated every 6–8 days at approximately 80% confluence. The 2nd passage (P2) of the cells was used if not otherwise stated.

hMSCs were characterized with respect to (a) the expression of surface antigens and (b) the ability to selectively differentiate into chondrogenic or osteogenic lineages in response to environmental stimuli, as follows. The expression of the following six surface antigens: CD14 (lipopolysaccharide receptor), CD31 (PECAM-1/endothelial cells), CD34 (sialomucin/hematopoietic progenitors), CD44 (hyaluronate receptor), CD71 (transferrin receptor/proliferating cells), and CD105 (endoglin), was characterized by Fluorescence Activated Cell Sorting (FACS) analysis, as in our previous studies [30,31]. Cells were detached with 0.05% (w/v) trypsin, pelleted, and resuspended at a concentration of 1×10^7 cells/ml. Fifty microliters of aliquots of the cell suspension was incubated (30 min on ice) with 2 μl of each of the following antibodies: anti-CD14 and anti-CD44 conjugated with fluoresceine isothiocyanate (CD14-FITC, CD44-FITC), anti-CD31 conjugated with phycoerythrin (CD31-PE), anti-CD34 and anti-CD71 conjugated with allophycocyanine (CD34-APC, CD71-APC), and anti-CD105 with a secondary rat-anti-mouse IgG-FITC antibody. Cells were washed, suspended in 100 μl of 2% formalin, and subjected to FACS analysis.

To assess the potential of hMSCs for osteogenic or chondrogenic differentiation, the cells were cultured in pellets in either *control medium* (DMEM supplemented with 10% FBS, Pen–Strep, and Fungizone), *chondrogenic medium* (control medium supplemented with 0.1 mM NEAA, 50 μg/ml ascorbic acid-2-phosphate, 10 nM dexamethasone, 5 μg/ml insulin, 5 ng/ml TGF-β1), or *osteogenic medium* (control medium supplemented with 50 μg/ml ascorbic acid-2-phosphate, 10 nM dexamethasone, 7 mM β-glycerolphosphate, and 1 μg/ml BMP-2). Cells were isolated from monolayers by trypsin and washed in PBS. Aliquots containing 2×10^5 cells were centrifuged at 300 *g* in 2 ml conical tubes and allowed to form compact cell pellets over 24 h in an incubator (5% CO_2, 37°C). Medium was changed every 2–3 days. After 4 weeks of culture, pellets were washed twice in PBS, fixed in 10% neutral buffered formalin (24 h at 4°C), embedded in paraffin, and sectioned (5 μm thick). Sections were stained for general evaluation (hematoxylin and eosin, H&E), the presence of glycosaminoglycan (GAG, safranin O/fast green), and mineralized tissue (according to von Kossa in 5% $AgNO_3$ for 1 h, exposed to a 60 W bulb and counterstained with fast red).

Tissue culture

For cultivation on scaffolds, P2 hMSCs were suspended in liquid BD Matrigel Basement Membrane Matrix (BD Biosciences, San Jose, CA) at a concentration of 1×10^6 cells per scaffold in 10 μl Matrigel while working on ice to prevent gelation. The cell suspension was seeded onto prewetted scaffolds and placed in an incubator (37°C, 5% CO_2) for 15 min to allow gel hardening. For cultivation in spinner flasks, these cell-seeded silk scaffolds were threaded onto needles embedded in the stoppers of the spinner flask (2 scaffolds on 4 needles per flask) as previously described [35,36]. Flasks were filled with 150 ml *osteogenic medium* (see above) and placed in a humidified incubator (37°C, 5% CO_2), with the side arm caps loosened to permit gas exchange and stirred with a magnetic bar at 60 rpm [31]. Medium was replaced at a rate of 50% every 2–3 days for 5 weeks of cultivation.

Biochemical analysis

After 5 weeks of cultivation in bioreactors, the tissue was punched into 5 mm diameter disks using a dermal punch (Miltey, Lake Success, NY). These scaffolds ($n=5$) were weighed and disintegrated using steel balls and a Minibead-beater (Biospec, Bartlesville, OK) in 0.5 ml 5% trichloroacetic acid in water. After a second extraction with 0.5 ml 5% trichloroacetic acid in water for 30 min and combination of the samples, calcium content was measured spectrophotometrically at 575 nm following the reaction with *o*-cresolphthalein complexone according to the manufacturer's protocol (Sigma, St. Louis, MO). For DNA analysis, 3–4 punched scaffolds were weighed, disintegrated using steel balls and a Minibead-beater in 0.2% Triton X-100 and 5 mM $MgCl_2$ solutions. DNA content was measured using the PicoGreen assay (Molecular Probes, Eugene, OR), according to the protocol of the manufacturer. Briefly, aliquots of the solutions prepared from the samples were measured fluorometrically at an excitation wavelength of 480 nm and an emission wavelength of 528 nm. Alkaline phosphatase activity (AP activity) was measured from aliquots as prepared for the DNA assay, using a biochemical assay from Sigma (St. Louis, MO), based on conversion of *p*-nitrophenyl phosphate to *p*-nitrophenol which was measured spectrophotometrically at 405 nm.

Operative procedure

An established, critically sized, femoral defect rat model was used in this study [37]. All procedures were approved by the operative institution's Animal Care and Use Committee. Adult, male athymic T-cell-deficient RH-rnu rats weighing 325–400 g were maintained under general anesthesia using isofluorane and oxygen delivered by mask. The animals received intramuscular injections of procaine penicillin antibiotic (200,000 IU/kg), once immediately prior to surgery and then once daily for 3 days. Buprenorphine (0.05 mg/kg) analgesic was administered subcutaneously once pre-operatively and then 3 times daily for approximately 48 h. Subsequent administration was based on the rat's disposition and was supplemented where indicated by the administration of subcutaneous ketoprofen (5 mg/kg once daily). The anesthetized rats were placed in lateral recumbency, and the uppermost hindlimb was shaved and aseptically prepared for surgery, prior to being draped. An approximately 25 mm long skin incision running the full length of the femur was created approximately 2 mm cranial to the bone. The subcutaneous tissues and facia were incised, the biceps femoris muscle was retracted posteriorly and the vastus muscle was retracted anteriorly. Self retaining retractors were used to expose the full length of the femur. A four-hole pre-drilled aluminum external fixator was placed over the lateral aspect of the exposed femur and used as a template to ensure appropriate positioning of four bicortical 0.9-mm diameter drill holes, which were created in the proximal (2) and distal (2) metaphysis of the femur. Four 1.1-mm external diameter self tapping threaded pins were then placed transcortically such that the pins extended approximately 0.5 mm beyond the trans cortex. Four small stab incisions were placed through the skin immediately caudal to the incision on the lateral aspect of the limb, allowing it to be placed over the pins. The external fixator was then placed over the pins and secured to them with miniscrews. A high speed dental drill was used to carefully create a 5-mm long full thickness osteo periosteal critical size defect in the mid-diaphysis which was subsequently packed with the test implant. Size 4-0 suture was used to appose the biceps femoris and vastus muscles around the defect, helping retain the implant in place, and a 4-0 subcuticular suture was used to close the subcutaneous space and skin.

Rats were euthanized 56 days after treatment. Both femora of each animal were harvested and either immediately frozen for biomechanical testing and micro-computed tomography (μCT) evaluation or placed in 4°C 4% paraformaldehyde for histological and immunohistochemical evaluation.

The rats were randomly assigned to one of four treatment groups (Table 1). Group I (6 rats) received predifferentiated hMSCs on silk scaffolds (pdHMSC/SS), group II (6 rats) received silk scaffolds seeded with undifferentiated hMSCs (udHMSC/SS), group III (6 rats) received unseeded silk scaffolds (SS), and in group IV, defects were left empty (control). Bone healing was monitored by weekly radiographs.

There are some serious complications associated with this model operating procedure, specifically, peri-anesthetic death (maybe related to rat strain), fracture of the parent bone during the technically very demanding fixation procedure or shortly thereafter, and pin tract infection that is usually manageable with cleaning and occasionally antibiotics. We encountered 15 euthanasia or deaths out of 54 prior to 8 weeks after operation, most of them occurred around the time of surgery.

Table 1
Description of the four treatment groups

Group	Abbreviation	Description
I	pdHMSC/SS	Human mesenchymal stem cells seeded on silk scaffolds and differentiated under osteogenic conditions for 5 weeks in spinner flasks prior to implantation
II	udHMSC/SS	Undifferentiated human mesenchymal stem cells seeded on silk scaffolds 1 day prior to implantation
III	SS	Silk scaffolds without cells
IV	control	No implant—empty defects

Histology and immunohistochemistry

Fixed and decalcified (12% EDTA, pH 7.0) femur explants were dehydrated in graded ethanol solutions and xylene, embedded in paraffin and cut into 3-μm-thick sections. For a general overview, sections were stained with H&E. Immunohistochemical studies were performed for bone sialoprotein (BSP) and collagen type I using a rabbit anti-bone sialoprotein II polyclonal antibody (Chemicon, Temecula, CA) and mouse anti-collagen type I monoclonal antibody (Sigma, St. Lois, MA), respectively. For collagen 1 antibody, sections were preincubated with 0.05% Pronase (Dako Cytomation, Baar, Switzerland) for 10 min and blocked two times 10 min with 3% H_2O_2 and with serum-free protein block (Dako Cytomation, Baar, Switzerland). The primary antibody was added to the slides at a dilution of 1:100 overnight, and after washing, an anti-mouse-peroxidase labeled polymer (EnVision+® System, K4001 Dako Cytomation, Baar, Switzerland) was applied for 30 min at room temperature. Samples were developed with an AEC Substrate Kit (Zymed Laboratories Inc., San Francisco, CA) under a light microscope. For BSP, the antibody was diluted 1:400, and the same procedure was followed except that there was no pronase pretreatment and the secondary antibody was an anti-rabbit peroxidase labeled polymer (EnVision+® System K4003 Dako Cytomation, Baar, Switzerland).

Micro-CT imaging and mechanical testing

Femoral defects were scanned using 55 kVp, 250 ms integration time, and 0.030 mm voxel side lengths (isotropic) on a micro-CT-40 system (Scanco Medical, Bassersdorf, Switzerland). Specimens were immersed in saline to homogenize the background the image and provide better contrast. The distance between the threaded pins was consistent, and this regularity aided in the scanning procedure. Micro-CT scans spanned the entire distance between the pins proximally and distally adjacent to the critical defect. After image reconstruction, volumes of interest (VOIs) were created for every specimen. VOIs were drawn contoured to the external boundary of the bone, beginning ten image slices distal to the fixator pin proximal to the defect and ending ten image slices proximal to the pin distal to the defect. VOIs were created only in regions where bone was present; in unhealed specimens, the gaps were excluded from the VOIs. Thus, morphometric analyses represented the geometry and bone morphology of the mineralized tissue in the region. Prior to morphometric analysis, a constrained Gaussian filter was used to suppress noise in the image (0.7 filter width) and images were thresholded. A previously described [33] adaptive, iterative threshold protocol was used that determined the threshold based on the characteristics of the image's histogram [38,39]. Performance tests (precision, accuracy, and stability of iterative algorithm) of this threshold approach on a variety of image types have proven it to be robust [40,41]. After thresholding, the total bone volume (BV), bone volume fraction (BV/TV), and average bone thickness (Th) were quantified. Bone volume was calculated by counting the total number of bone voxels and multiplying by their known volume. The bone volume fraction was calculated as the ratio of the bone voxels to the total number of voxels (bone and non-bone voxels after thresholding). Bone thickness was measured in three dimensions in accordance with the method established by Hildebrand and Ruegsegger [42].

Both ends of specimens were embedded in blocks of polymethylmethacrylate (PMMA) to provide gripping points for torsional testing. The specimens were kept wet during the PMMA exothermic curing process to avoid drying. Mechanical testing was performed using a torsion testing system that applies a force couple via cables attached to a pulley fixed to the top of a cylindrical bone specimen such that the axis of rotation of the pulley is coincident with the geometric neutral axis of the cylindrical bone specimen. A module containing a roller clutch, an XY sliding surface, and coupling cables was mounted to an MTS200 screw axis load frame (MTS, Saint Paul, MN, USA) for the application of torque. The module maintains the prescribed torque on the specimen when it is removed from the load frame. Torsional testing was performed using a strain rate of 5 rad/min, and the data were collected with a LabVIEW (National Instruments, Austin, TX) acquisition system. Maximum torsional displacement (rad) and load (N) and maximum torque (Nm) were measured for each specimen. Additionally, torsional stiffness (N.m/rad) was calculated from the slope fit to the linear portion of the torsional load displacement curve.

Statistical analysis

For statistical significance, samples were evaluated using a Student's *t* test as well as ANOVA where appropriate. ANOVA was followed by a post hoc assessment

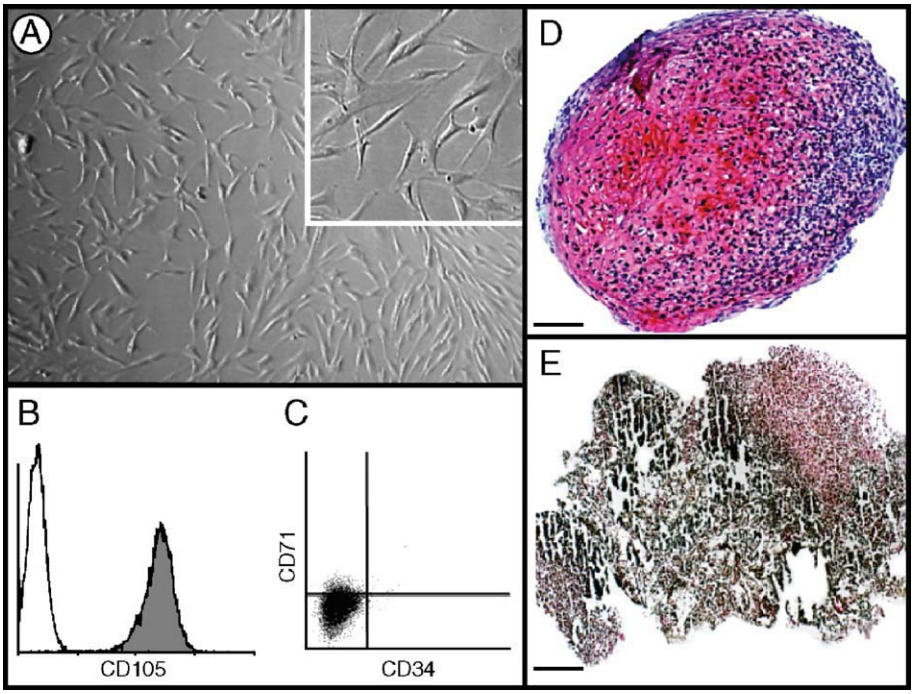

Fig. 1. Characterization of human mesenchymal stem cells. (A) Cells had a fibroblast-like morphology and presented the (B) CD105 and (C) CD71, but not the CD34 antigen on their surfaces, respectively. Pellet culture in chondrogenic medium (D) resulted in the deposition of an intensively red staining matrix with safranin O. Pellets cultured in osteogenic medium and stained with von Kossa displayed black staining. Magnifications (A) 40× and 100× (insert), (D, E) scale bar length = 100 μm. (For interpretation of the references to colour in this figure legend, the reader is referred to the web version of this article.)

using the Tukey HSD method. Differences were considered significant when equal or less than $P=0.05$.

Results

Cell characteristics and bioreactor culture

The cells were adherent to tissue culture plastic after about 6 h and showed a fibroblast-like morphology (Fig. 1A). Their surface antigen pattern was $CD105^+$ (Fig. 1B), $CD71^+$, and $CD34^-$ (Fig. 1C) and $CD44^+$, $CD14^-$, and $CD31^-$ (data not shown). After 5 weeks of pellet culture in chondrogenic medium, the cells deposited an intensely red staining matrix with safranin O (Fig. 1D), indicating deposition of extracellular glycosaminoglycans. The culture in osteogenic medium resulted in the formation of a black staining matrix in a von Kossa staining (Fig. 1E) noting for mineralized extracellular matrix. In control medium, no positive safranin O or von Kossa staining was observed (data not shown).

When cells were seeded on silk fibroin scaffolds (SS) and cultured in spinner flask bioreactors with osteogenic medium for 5 weeks, alkaline phosphatase activity followed an undulating pattern, with significantly higher activity after 2 and 4 weeks, when compared to weeks 1 and 3 (Fig. 2A; $P<0.05$ or <0.01). Mineralization determined by calcium assay started between week 1 and 2 ($P<0.01$) and continued to increase between week 3 and 4 ($P<0.01$). No increase in mineralization was observed between week 4 and 5 (Fig. 2B).

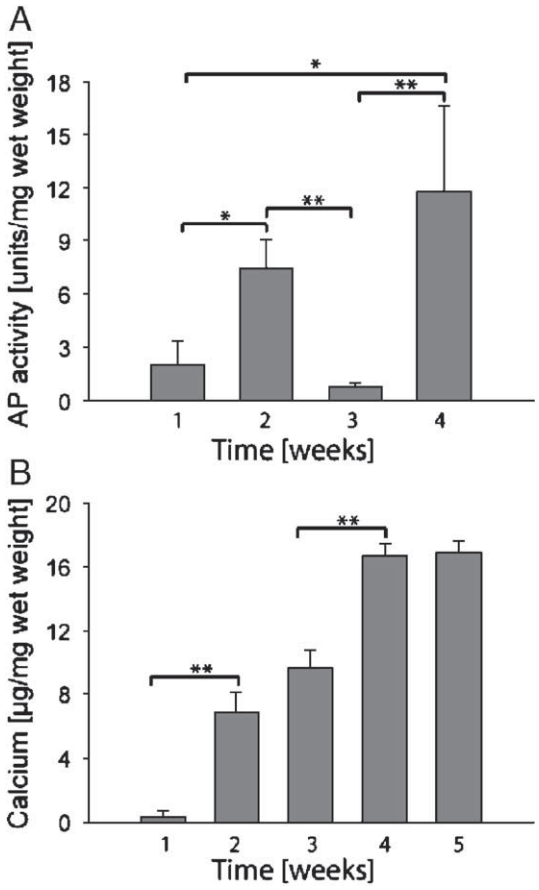

Fig. 2. (A) Alkaline phosphatase activity and (B) calcium deposition over time from silk scaffolds cultured in bioreactors for 5 weeks (**$P<0.01$, *$P<0.05$; $n=5$ per group).

In vivo studies

The implantation of pdHMSC/SS (group I, Table 1) into critical size femoral defects resulted in good integration of the implant with the fracture ends at 8 weeks post-surgery. Substantial new bone formation (25–40%) was observed, with more cortical bone in the outer implant zones and more interconnected, woven bone in the centers, as shown with H&E staining (Fig. 3A). Positive staining for bone sialoprotein (BSP) and collagen type I (data not shown) was found in the newly formed matrix of actively bone-forming sites. Aside from long cells with fibroblastic morphology and stranded connective tissue, the formation of new woven bone was observed (Fig. 3A, insert). No apparent signs of silk scaffold degradation were observed, as indicated by the smooth lattice surfaces, although foreign body cells were present (Fig. 3A).

The implantation of udHMSC/SS (group II, Table 1) resulted in the formation of a fibroblast tissue throughout the implantation zone (Fig. 3B), with some few capillaries randomly dispersed through the implant's lattice (Fig. 3B, insert). Bone formation was mainly observed at the defect margins with the parent bone but not at the center of the defect. Moderate positive staining for BSP and type I collagen was mainly found at the interface between the defect border and the newly formed bone as well as few and randomly clusters distributed throughout the matrix (data not shown). A higher number of foreign body cells than in group I were present in the defect zone, but the SS seemed well embedded in the cell- and extracellular-matrix-rich environment.

Defects treated with unseeded scaffolds SS (group III, Table 1) developed a dense cellular network in the vicinity of the defect borders and appositional to the scaffold lattice (Fig. 3C). Substantially fewer cells were found in the defect center, and scaffold interaction with the host tissue was weaker as observed in groups I and II and as indicated by lower cell numbers and void spaces at the host–implant interface (Fig. 3C). Immunohistochemistry showed positive staining for both BSP and type I collagen within the matrix and cells with a fibroblastic morphology within the scaffold center, whereas loosely connected cells with a connective-tissue-like morphology stained positive only for type I collagen but not BSP. The small amounts of new woven bone stained positive only for BSP.

Tissue formation in the empty defects (group IV, Table 1) was confined to the defect margins with parent bone, with some clusters of non-bone-forming cells found in more distal regions (Fig. 3D and insert). These clusters did stain only faintly for BSP and positive for type I collagen, respectively.

The morphology of the formed bone was evaluated using µCT (Fig. 4). In general, defects treated with pdHMSC/SS (group I) were spanned by cortical-like bone in the outer zones and a cancellous-like but irregularly and loosely connected bone tissue within the defect center. The defects in three of the six rats were completely bridged with no apparent cracks, two by small

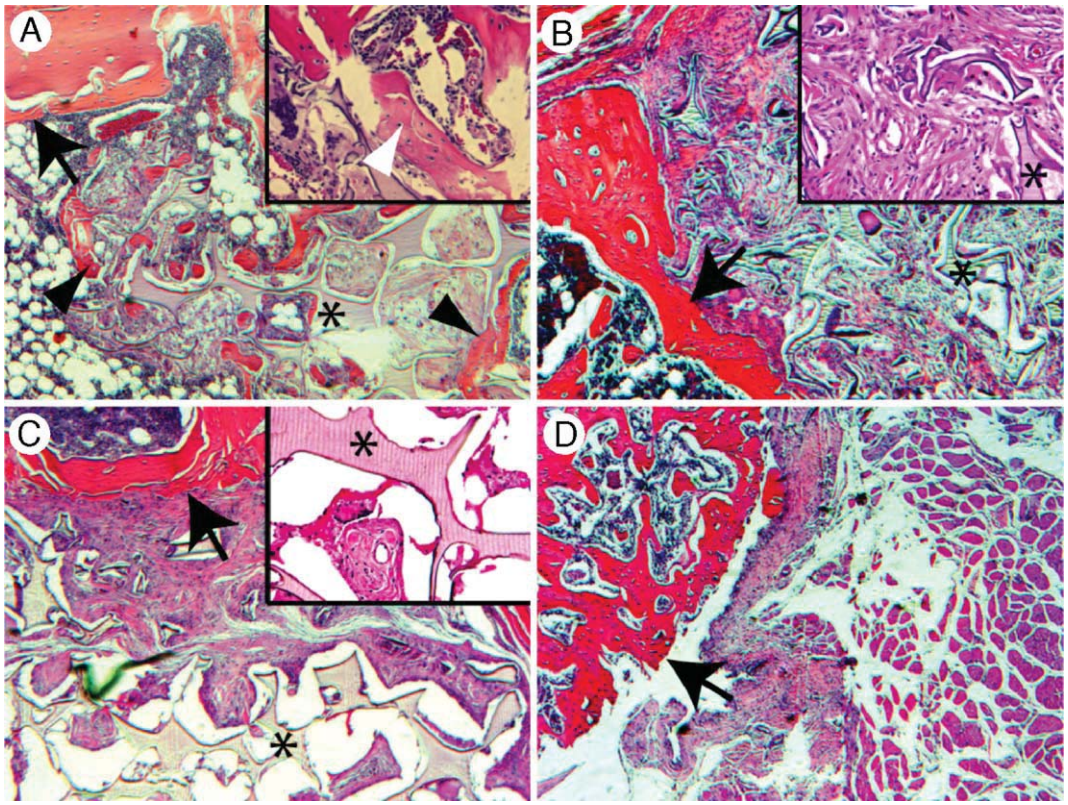

Fig. 3. Histological cross-sections taken from rat critical size femoral defects 8 weeks after surgery. (A) pdHMSC on silk scaffolds, (B) silk scaffolds seeded with udHMSC, (C) unseeded silk scaffolds, and (D) untreated (control) defects. Magnification 50×, inserts 100×. Asterisks indicate silk scaffold, arrows the fracture ends, arrowheads newly formed bone within the defect.

in the center of the implant and along the line of the stacked implant discs and one by large cracks spanning throughout the defect zone. The implantation of udHMSC/SS (group II) resulted in bone formation at the defect margins with parent bone and some minor formation within the defect center, however, no bridging of the defect was observed. Finally, no bone formation was apparent for defects treated with unseeded SS (group III) or empty control defects (group IV).

Morphometric analysis based on the tomographic evaluations quantified the qualitative observations previously detailed. Significantly more bone volume was observed in group I as compared to all other treatment groups ($P<0.01$; Fig. 5A). The ratio of bone volume to total volume, as an indicator of the relative amount of formed bone, was significantly higher for group-I-treated defects when compared to all other groups ($P<0.01$; Fig. 5B). The thickness of the bone formed was consistent among groups, with apparently high standard deviations (data not shown).

The defects were mechanically characterized (Fig. 6). The maximal load before failure was significantly higher for group I when compared to groups II ($P<0.05$) and III ($P<0.01$). The implantation of udHMSC/SS (group II) resulted in significantly higher maximal load levels when compared to group III ($P<0.01$). Similarly, the maximal torque was higher for pdHMSC/SS (group I) when compared to groups II ($P<0.05$) and III ($P<0.01$), respectively. Maximal torque was significantly higher for group II when compared to the SS (group III) ($P<0.01$). The total stiffness of the defects was higher for the pdHMSC/SS (group I) when compared to group III ($P<0.01$), but no significant differences were observed between group I and II or between group II and III.

Discussion

The goal of the present study was to evaluate a new protein-based biomaterial scaffold system with mechanically robust and durable properties upon implantation into long bone and critically sized femoral defects. A tissue-engineered trabecular bone-like tissue was generated from pdHMSC/SS (group I, Table 1) which were pre-cultured in osteogenic medium for 5 weeks. These implants were inserted into the defect site, and osteogenesis was compared to defects treated with udHMSC seeded silk scaffolds, those not pre-cultured in osteogenic medium (group II, Table 1), unseeded silk scaffolds (group III, Table 1), and untreated control defects (empty, group IV, Table 1).

Silk fibroin, the structural, hydrophobic, and approximately 370 kDa protein isolated from the cocoon of *B. mori* [43–46] that has emerged as a novel substrate for engineering biomaterials, has proven to be biocompatible [22,33], offers distinguishing mechanical properties when compared to other naturally derived or degradable polymeric biomaterials [47], and exhibits low inflammatory response [21,22].

Stem cells are believed to be one of the most interesting cell sources for tissue engineering, particularly for the (re)generation

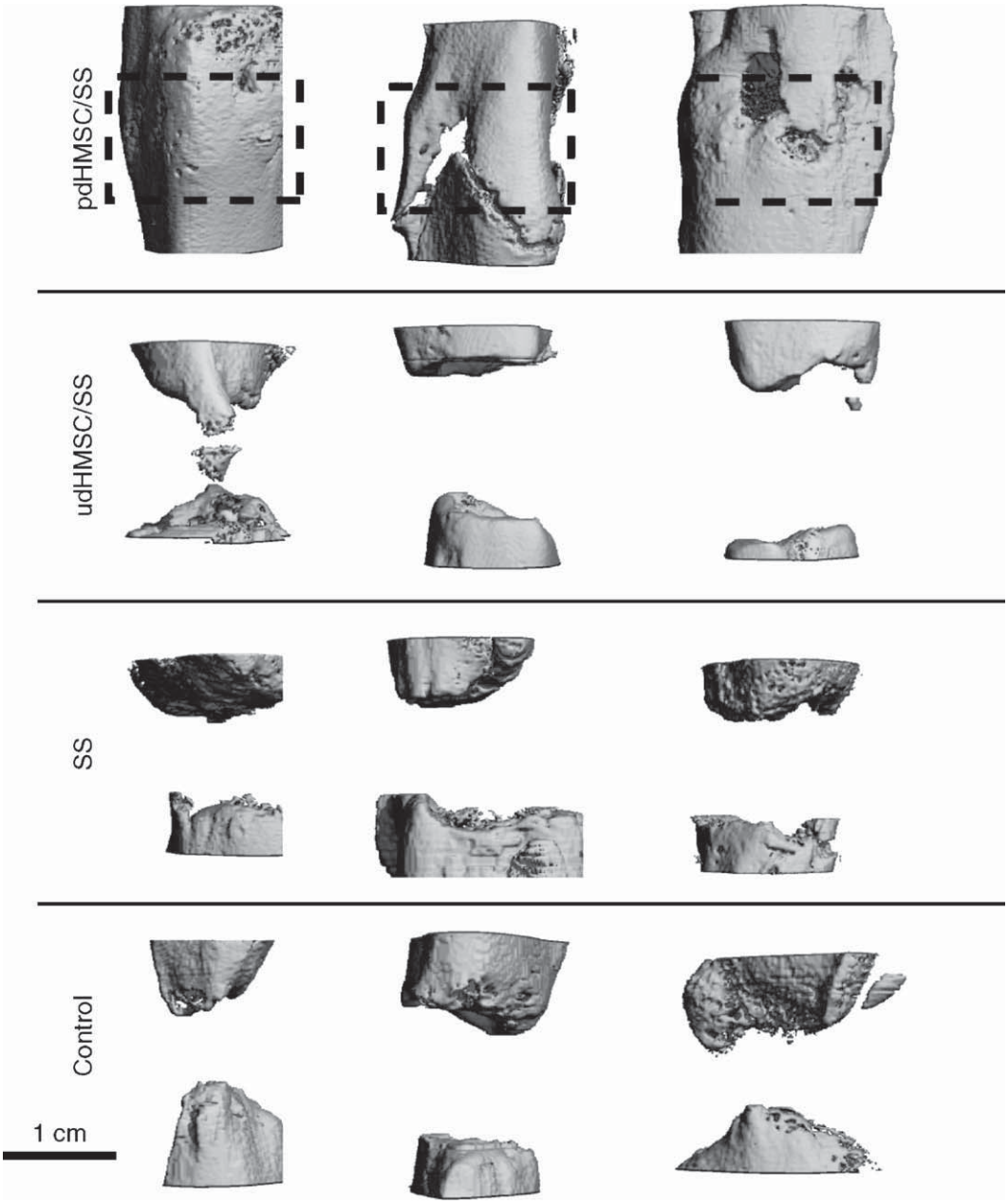

Fig. 4. Micro-computed tomography from three representative rat critical size femoral defects 8 weeks after surgery; pdHMSC grown 5 weeks on silk scaffolds (group I), silk scaffolds seeded with udHMSC (group II), unseeded silk scaffolds (group III), and untreated (control) defects (group IV). The dotted box approximately indicates the original defect zone.

of bone tissue. This is due to characteristics inherent in stem cells such as (i) a high proliferation capacity, (ii) ability for self-renewal, (iii) multilineage differentiation and, therefore, potential for the repair of various tissues [48–52]. The cells used in this study were characterized as stem cells based on their surface markers as well as the multipotent and selective differentiation outcomes shown to bone or cartilage. Silk fibroin scaffolds seeded with hMSCs and cultured in osteogenic medium in spinner flask bioreactors generated bone-like biochemical responses as typically observed for mesenchymal cells on other biomaterials [31,32,53]. The high degree of mineralization observed, beginning between weeks 1 and 2 post-seeding, is evidence of the strong osteogenic commitment of the hMSCs on silk scaffolds and in the presence of BMP-2 (one of the osteogenic media components).

Substantial differences were observed in vivo in bone healing between pdHMSC/SS (group I), udHMSC/SS (group II) and the SS (group III). The implantation of pdHMSC/SS into the defect resulted in substantial and homogenous bridging of the majority of defects (Figs. 3, 4), significantly ($P<0.01$) higher bone volumes and bone volumes per trabecular volume (which indicates a shift from trabecular to cortical bone), and a substantial increase in mechanical properties when compared to the other groups. The premineralization of the silk scaffolds appears to be important in

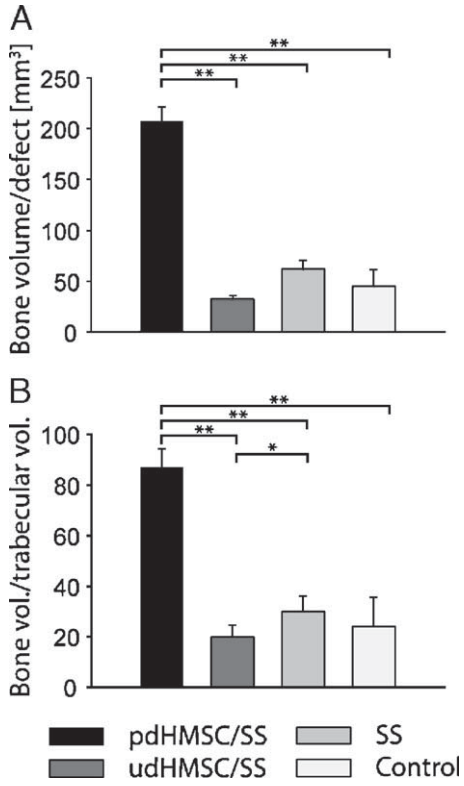

Fig. 5. Morphometric analysis of new bone formation from rat critical size femoral defects 8 weeks after surgery and treated with pdHMSC grown for 5 weeks on silk scaffolds (group I), silk scaffolds seeded with udHMSC (group II), unseeded silk scaffolds (group III), and untreated (control) defects (group IV). (A) Bone volume per defect, and (B) bone volume normalized to the trabecular volume (**$P<0.01$, *$P<0.05$).

overall bone restoration in vivo. Thus, future studies should also address the relative contribution of mineralization on silk fibroin scaffolds related to osteoconductivity with and without the presence of hMSCs during implantation. Although bone formation within the defect zone was restricted to the defect margins, the udHMSC seeded scaffolds (group II) resulted in significantly ($P<0.01$) higher maximal load and torque when compared to unseeded SS (group III). This may be due to the formation of a dense cellular- and matrix-rich network supported by the silk scaffolds between the host bone and the scaffold center, fixing the stacked scaffold disks in place and thereby resulting in a more stabilized mechanical environment. However, the mechanical data were presented to provide a relative strength profile across study groups. This must be noted as the femurs were fixed before measurements, instead of most biomechanical studies. We have not tested if the fixation altered the mechanical properties of bone. Therefore, one should be careful to compare the presented data to normal unfixed rat bones since only the relative strength of specimens across different groups is of consequence in this study. As part of the morphometric analysis of the engineered bone-like tissue, we evaluated the bone thickness using an algorithm validated for trabecular bone (data not shown). However, the repair side consisted of complex, inhomogenous structures other than trabecular bone (Fig. 3). The validation for the algorithm used was not validated for the type of tissue formed in the defect site. Consistently, our data showed a large variation. The validation of algorithms provided should be carefully evaluated for the intended application.

The gold standard of bone replacement is autograft bone or bone that has been harvested from another anatomic location in the same individual and then inserted into the fracture zone [8,54]. The advantage of this approach is the combined transplantation of autologous cells, scaffold material, and growth factors stored within the matrix [55,56]. However, harvesting autologous bone is associated with second site morbidity and hampered by insufficient amounts of collected bone substance to fill the entire defect [57]. Apart from other options such as the use of allograft bone, which is associated with the risk of disease transmission or immune rejection, metals and ceramics are used to treat larger defects [58]. Metals provide instant mechanical stability but are associated with poor overall integration and can fail because of

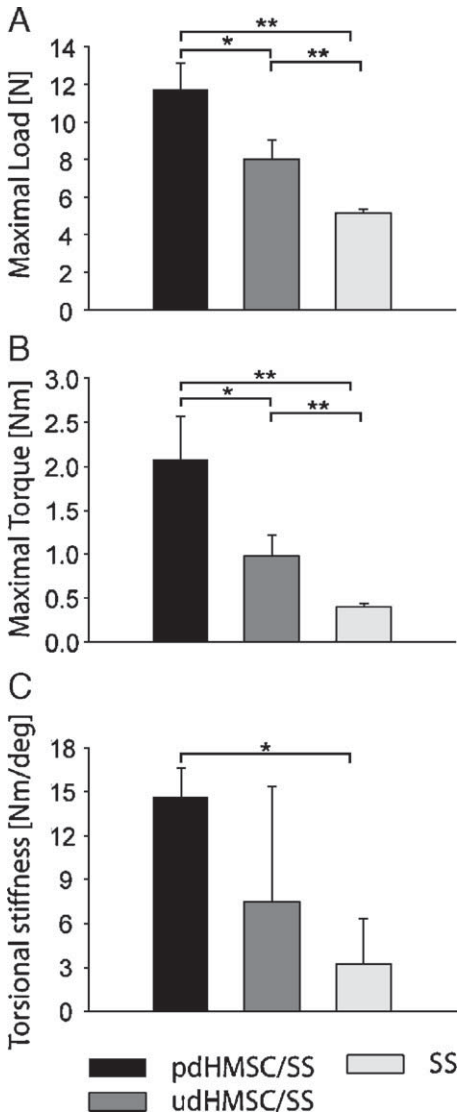

Fig. 6. Mechanical features of rat critical size femoral defects 8 weeks after surgery and treated with pdHMSC for 5 weeks on silk scaffolds (group I), silk scaffolds seeded with udHMSC (group II), and unseeded silk scaffolds (group III). (A) Maximal load before break, (B) maximal torque, and (C) torsional stiffness (**$P<0.01$, *$P<0.05$).

infection or due to fatigue loading [7]. Ceramics generally have very low tensile strength, are brittle, and cannot be used in locations of significant torsion such as long bones [3,4,59–61]. Alternatively, biomaterials such as type I collagen base implants are frequently used but have limitations related to rapid biodegradation or – when stabilized through cross-linking – foreign body responses and uncontrolled calcification [62,63].

The combined use of an organic template based on silk fibroin and hMSCs predifferentiated in bioreactors with osteogenic medium (group I) provides an alternative route for future treatment scenarios of larger femoral defects. In this study, the filling of the defect was achieved by stacking five silk scaffolds, each of which was individually engineered, to result in good bone integration. In vivo bone formation resulted in a good formation of bone between the stacked disks and the fracture ends, respectively. However, the engineering of a pdHMSC/SS using a single block of silk instead of staggered disks should further improve the mechanical properties, integrity, and safety. However, this is currently challenging due to limitations in nutrient and gas transport during predifferentiation in vitro. Bone is a highly vascularized and metabolically active tissue and especially prone to low oxygen tensions, quickly resulting in necrotic responses. These limitations curtail current tissue engineering approaches, resulting in bone thicknesses limited to approximately 500 μm to 1 mm [32,64]. Future studies aiming at increased mass and gas transport in the scaffolds when cultured in vitro are important and could be addressed through novel designs for the bioreactors, scaffolds, and medium used in the process (e.g., by addition of oxygen binding molecules mimicking the function of hemoglobin [64]).

Tissue engineering can provide adequate bone replacement resulting in full recovery of the patient [65]. The results of the present study indicate that the implantation of tissue-engineered bone on silk scaffolds was suitable for this application because it leads the way to bridging of critical size defects with newly formed functional bone. This was also reflected in mechanical properties, with group I exceeding all other groups in terms of maximal load before failure, maximal torque, and torsional stiffness. Although bone formation was limited in groups II and III, some mechanical integrity was achieved due to the presence of the silk and some fixation due to the invasion of fibrous tissues into the implant materials. The osteoinduction achieved in group I rats resulted in complete bridging of femoral, segmental critically sized defects with a callus on the outside and around 30% newly formed woven bone tissue inside the defect. These findings encourage the continued investigation of potential use of silks as a mechanically stable and robust scaffold for tissue-engineered constructs and load bearing bones. Future studies should be conducted to validate the effectiveness of this procedure in larger animals.

Acknowledgments

This work was supported by the German Alexander von Humboldt Foundation (Feodor-Lynen fellowship to LM), the National Institutes of Health (DE13405-04 and EB002520 to DK), and the National Science Foundation (DMR-0090384 to DK) and the association for orthopedic research (ETH Zurich, TH Gesuch). We thank Katie Zlinszky for technical assistance in immunohistological stainings and Nipun Patel for help with micro-CT as well as the mechanical evaluations.

References

[1] Reginster JY. The prevalence and burden of arthritis. Rheumatology (Oxford) 2002;41(Supp 1):3–6.
[2] Lysaght MJ, Reyes J. The growth of tissue engineering. Tissue Eng 2001;7:485–93.
[3] McAndrew MP, Gorman PW, Lange TA. Tricalcium phosphate as a bone graft substitute in trauma: preliminary report. J Orthop Trauma 1988;2:333–9.
[4] Heuer AH, Fink DJ, Laraia VJ, Arias JL, Calvert PD, Kendall K, et al. Innovative materials processing strategies: a biomimetic approach. Science 1992;255:1098–105.
[5] Cornell CN, Lane JM. Current understanding of osteoconduction in bone regeneration. Clin Orthop 1998:S267–73.
[6] Hollinger JO, Brekke J, Gruskin E, Lee D. Role of bone substitutes. Clin Orthop 1996:55–65.
[7] Suh H. Recent advances in biomaterials. Yonsei Med J 1998;39:87–96.
[8] Einhorn TA. Enhancement of fracture-healing [see comments]. J Bone Joint Surg Am Vol 1995;77:940–56.
[9] Horowitz MC, Friedlaender GE. Immunologic aspects of bone transplantation. A rationale for future studies. Orthop Clin North Am 1987;18:227–33.
[10] Bos GD, Goldberg VM, Zika JM, Heiple KG, Powell AE. Immune responses of rats to frozen bone allografts. J Bone Joint Surg Am 1983;65:239–46.
[11] Hollinger JO, Leong K. Poly(alpha-hydroxy acids): carriers for bone morphogenetic proteins. Biomaterials 1996;17:187–94.
[12] Albrektsson T, Johansson C. Osteoinduction, osteoconduction and osseointegration. Eur Spine J 2001;10(Suppl 2):S96–S101.
[13] DeLustro F, Dasch J, Keefe J, Ellingsworth L. Immune responses to allogeneic and xenogeneic implants of collagen and collagen derivatives. Clin Orthop 1990:263–79.
[14] Luginbuehl V, Meinel L, Merkle HP, Gander B. Localized delivery of growth factors for bone repair. Eur J Pharm Biopharm 2004;58:197–208.
[15] Ohgushi H, Okumura M, Masuhara K, Goldberg VM, Davy DT, Caplan AI. Calcium phosphate block ceramic with bone marrow cells in a rat long bone defect. In: Yamamuro T, Hench L, Wilson J, editors. CRC handbook of bioactive ceramics, vol. 2. Boca Raton, FL: CRC Press; 1992. p. 235–8.
[16] Petite H, Viateau V, Bensaid W, Meunier A, de Pollak C, Bourguignon M, et al. Tissue-engineered bone regeneration. Nat Biotechnol 2000;18:959–63.
[17] Athanasiou KA, Niederauer GG, Agrawal CM. Sterilization, toxicity, biocompatibility and clinical applications of polylactic acid/polyglycolic acid copolymers. Biomaterials 1996;17:93–102.
[18] Harris LD, Kim BS, Mooney DJ. Open pore biodegradable matrices formed with gas foaming. J Biomed Mater Res 1998;42:396–402.
[19] Rossitch Jr E, Bullard DE, Oakes WJ. Delayed foreign-body reaction to silk sutures in pediatric neurosurgical patients. Childs Nerv Syst 1987;3:375–8.
[20] Santin M, Motta A, Freddi G, Cannas M. In vitro evaluation of the inflammatory potential of the silk fibroin. J Biomed Mater Res 1999;46:382–9.
[21] Panilaitis B, Altman GH, Chen J, Hyoung-Joon J, Karageorgiou V, Kaplan DL. Macrophage responses to silk. Biomaterials 2003;24:3079–85.
[22] Meinel L, Hofmann S, Karageorgiou V, Kirker-Head C, McCool J, Gronowicz G, et al. The inflammatory responses to silk films in vitro and in vivo. Biomaterials 2005;26:147–55.
[23] Sofia S, McCarthy MB, Gronowicz G, Kaplan DL. Functionalized silk-based biomaterials for bone formation. J Biomed Mater Res 2001;54:139–48.
[24] Halsted W. The employment of fine silk in preference to catgut and the advantage of transfixing tissues and vessels in controlling hemorrhage. Ann Surg 1892;16:505.
[25] Asakura T, Kaplan DL. Silk production and processing. In: Arutzen CJ, editor. Encyclopedia of agriculture science, vol. 4. New York: Academic; 1994. p. 1–11.
[26] Altman GH, Horan RL, Lu HH, Moreau J, Martin I, Richmond JC, et al. Silk matrix for tissue engineered anterior cruciate ligaments. Biomaterials 2002;23:4131–41.

[27] Jin HJ, Kaplan DL. Mechanism of silk processing in insects and spiders. Nature 2003;424:1057–61.
[28] Nazarov R, Jin HJ, Kaplan DL. Porous 3-D scaffolds from regenerated silk fibroin. Biomacromolecules 2004;5:718–26.
[29] Kim UJ, Park J, Li C, Jin HJ, Valluzzi R, Kaplan DL. Structure and properties of silk hydrogels. Biomacromolecules 2004;5:786–92.
[30] Meinel L, Hofmann S, Karageorgiou V, Zichner L, Langer R, Kaplan D, et al. Engineering cartilage-like tissue using human mesenchymal stem cells and silk protein scaffolds. Biotechnol Bioeng 2004;88:379–91.
[31] Meinel L, Karageorgiou V, Fajardo R, Snyder B, Shinde-Patil V, Zichner L, et al. Bone tissue engineering using human mesenchymal stem cells: effects of scaffold material and medium flow. Ann Biomed Eng 2004;32:112–22.
[32] Meinel L, Karageorgiou V, Hofmann S, Fajardo R, Snyder B, Li C, et al. Engineering bone-like tissue in vitro using human bone marrow stem cells and silk scaffolds. J Biomed Mater Res 2004;71A:25.
[33] Meinel L, Fajardo R, Hofmann S, Langer R, Chen J, Snyder B, et al. Silk implants for the healing of critical size bone defects. Bone 2005;37: 688–98.
[34] L. Meinel, S. Hofmann, O. Betz, R. Fajardo, C. Evans, G. Vunjak-Novakovic, et al., Bone engineering with human mesenchymal stem cells on silk: a comparison of adenoviral gene and protein therapy. Submitted for publication.
[35] Vunjak-Novakovic G, Martin I, Obradovic B, Treppo S, Grodzinsky AJ, Langer R, et al. Bioreactor cultivation conditions modulate the composition and mechanical properties of tissue-engineered cartilage. J Orthop Res 1999;17:130–8.
[36] Vunjak-Novakovic G, Obradovic B, Martin I, Bursac PM, Langer R, Freed LE. Dynamic cell seeding of polymer scaffolds for cartilage tissue engineering. Biotechnol Prog 1998;14:193–202.
[37] Einhorn TA, Lane JM, Burstein AH, Kopman CR, Vigorita VJ. The healing of segmental bone defects induced by demineralized bone matrix. A radiographic and biomechanical study. J Bone Joint Surg Am 1984;66:274–9.
[38] Ridler TW, Calvard S. Picture thresholding using an iterative selection method. IEEE Trans Syst Man Cybern 1978;8:630–2.
[39] Trussell HJ. Picture thresholding using an iterative selection method—comments. IEEE Trans Syst Man Cybern 1979;9:311.
[40] Glasbey CA. An analysis of histogram-based thresholding algorithms. CVGIP Graph Models Image Process 1993;55:532–7.
[41] Leung CK, Lam FK. Performance analysis for a class of iterative image thresholding algorithms. Pattern Recogn 1996;29:1523–30.
[42] Hildebrand T, Laib A, Muller R, Dequeker J, Ruegsegger P. Direct three-dimensional morphometric analysis of human cancellous bone: microstructural data from spine, femur, iliac crest, and calcaneus. J Bone Miner Res 1999;14:1167–74.
[43] Dewair M, Baur X, Ziegler K. Use of immunoblot technique for detection of human IgE and IgG antibodies to individual silk proteins. J Allergy Clin Immunol 1985;76:537–42.
[44] Craig CL, Hsu M, Kaplan D, Pierce NE. A comparison of the composition of silk proteins produced by spiders and insects. Int J Biol Macromol 1999;24:109–18.
[45] Inoue S, Tanaka K, Arisaka F, Kimura S, Ohtomo K, Mizuno S. Silk fibroin of *Bombyx mori* is secreted, assembling a high molecular mass elementary unit consisting of H-chain, L-chain, and P25, with a 6:6:1 molar ratio. J Biol Chem 2000;275:40517–28.
[46] Tanaka K, Inoue S, Mizuno S. Hydrophobic interaction of P25, containing Asn-linked oligosaccharide chains, with the H–L complex of silk fibroin produced by *Bombyx mori*. Insect Biochem Mol Biol 1999;29:269–76.
[47] Cunniff PM, Fossey SA, Auerbach MA, Song JW, Kaplan DJ, Adams WW, et al. Mechanical and thermal properties of the dragline silk from the spider *Nephila claviceps*. Polym Adv Technol 1994;5:401–10.
[48] Service RF. Tissue engineers build new bone [news]. Science 2000;289: 1498–500.
[49] Jaiswal N, Haynesworth SE, Caplan AI, Bruder SP. Osteogenic differentiation of purified, culture-expanded human mesenchymal stem cells in vitro. J Cell Biochem 1997;64:295–312.
[50] Aubin JE. Bone stem cells. J Cell Biochem Suppl 1998;30–31:73–82.
[51] Bruder SP, Fink DJ, Caplan AI. Mesenchymal stem cells in bone development, bone repair, and skeletal regeneration therapy. J Cell Biochem 1994;56:283–94.
[52] Friedenstein AJ, Chailakhyan RK, Gerasimov UV. Bone marrow osteogenic stem cells: in vitro cultivation and transplantation in diffusion chambers. Cell Tissue Kinet 1987;20:263–72.
[53] Choong PF, Martin TJ, Ng KW. Effects of ascorbic acid, calcitriol, and retinoic acid on the differentiation of preosteoblasts. J Orthop Res 1993;11:638–47.
[54] Johnson EE, Urist MR, Finerman GA. Repair of segmental defects of the tibia with cancellous bone grafts augmented with human bone morphogenetic protein. A preliminary report. Clin Orthop 1988:249–57.
[55] Eiselt P, Kim BS, Chacko B, Isenberg B, Peters MC, Greene KG, et al. Development of technologies aiding large-tissue engineering. Biotechnol Prog 1998;14:134–40.
[56] Nade S, Burwell RG. Decalcified bone as a substrate for osteogenesis. An appraisal of the interrelation of bone and marrow in combined grafts. J Bone Joint Surg Am Br 1977;59:189–96.
[57] Einhorn TA, Lee CA. Bone regeneration: new findings and potential clinical applications. J Am Acad Orthop Surg 2001;9:157–65.
[58] Kokubo T, Kim HM, Kawashita M, Nakamura T. Bioactive metals: preparation and properties. J Mater Sci Mater Med 2004;15:99–107.
[59] Dennis JE, Haynesworth SE, Young RG, Caplan AI. Osteogenesis in marrow-derived mesenchymal cell porous ceramic composites transplanted subcutaneously: effect of fibronectin and laminin on cell retention and rate of osteogenic expression. Cell Transplant 1992;1:23–32.
[60] Klein CP, Driessen AA, de Groot K. Relationship between the degradation behaviour of calcium phosphate ceramics and their physical–chemical characteristics and ultrastructural geometry. Biomaterials 1984;5:157–60.
[61] Driessen AA, Klein CP, de Groot K. Preparation and some properties of sintered beta-whitlockite. Biomaterials 1982;3:113–6.
[62] Nimni ME, Cheung D, Strates B, Kodama M, Sheikh K. Chemically modified collagen: a natural biomaterial for tissue replacement. J Biomed Mater Res 1987;21:741–71.
[63] Srivastava S, Gorham SD, French DA, Shivas AA, Courtney JM. In vivo evaluation and comparison of collagen, acetylated collagen and collagen/glycosaminoglycan composite films and sponges as candidate biomaterials. Biomaterials 1990;11:155–61.
[64] Vunjak-Novakovic G, Meinel L, Altman G, Kaplan D. Bioreactor cultivation of osteochondral grafts. Orthod Craniofac Res 2005;8:209–18.
[65] Langer R, Vacanti JP. Tissue engineering. Science 1993;260:920–6.